Contents lists available at ScienceDirect

Journal of Drug Delivery Science and Technology

journal homepage: www.elsevier.com

Formulation and characterization of mucoadhesive controlled release matrix tablets of captopril

J. Saurí [a, *], M. Zachariah [c], R. Macovez [c], J. Ll. Tamarit [c], D. Millán [d], M. Suñé-Pou [a], E. García-Montoya [a, b], P. Pérez-Lozano [a, b], M. Miñarro [a, b], J.R. Ticó [a, b], J.M. Suñé-Negre [a, b]

[a] Pharmacy and Pharmaceutical Technology Department, Universitat de Barcelona, Barcelona, Spain
[b] IDIBELL-UB Research Group: Pharmacotherapy, Pharmacogenomics & Pharmaceutical Technology, Barcelona, Spain
[c] Group of Characterization of Materials, Department of Physics, Universitat Politècnica de Catalunya, Barcelona, Spain
[d] Lab. Kern Pharma, Barcelona, Spain

ARTICLE INFO

Article history:
Received 17 January 2017
Received in revised form 12 March 2017
Accepted 12 March 2017
Available online xxx

Keywords:
Mucoadhesion
Drug release
Hydrophilic matrix tablets
Quality by design
Broadband dielectric spectroscopy

ABSTRACT

The purpose of this study is to characterize controlled release matrix tablets of captopril and to find out the physicochemical properties that have an effect on the mucoadhesion process. The hydrophilic matrix tablets contain captopril, microcrystalline cellulose, barium sulfate, ascorbic acid, ethylcellulose N100, hydroxypropylmethylcellulose K15M, talc, magnesium stearate and colloidal silicon dioxide. The physicochemical properties of the formulations have been characterized using confocal microscopy, contact angle, and scanning electron microscopy. The potential mucoadhesion capabilities of the formulations were assessed measuring the surface free energy, the polar and dispersive forces, the spreading coefficients, the surface roughness, and the network structure of the hydrophilic matrix tablets. The results show that when the concentration of HPMC K15M increases, the spreading coefficients of polymer over mucus and mucus over polymer are more positive, thus increasing the contact between the matrix tablets with the mucus layer. The formulation that contains 15% of HPMC K15M is the formulation that presents a greater swelling capacity, a greater increase in surface roughness, and larger pores within the matrix. This formulation has a higher chain mobility and more free macromolecular chains able to diffuse in the mucus layer. Therefore, this formulation has the greatest potential mucoadhesion capability.

1. Introduction

Mucosal drug delivery offers various advantages including the ability to target local disorders in order to reduce systemic dosage thereby minimizing side effects, and to promote systemic drug delivery through various routes of administration [1].

Mucoadhesion has been widely promoted as a way of achieving site-specific drug delivery through the incorporation of mucoadhesive hydrophilic polymers within pharmaceutical formulations along with the active pharmaceutical ingredient (API) [2].

The total phenomenon of mucoadhesion is likely to be a combined result of all the phenomena considered by the different theories. Some researchers prefer to divide the mucoadhesion process into sequential phases, each of which is associated with a different mucoadhesion mechanism [3,4]. First, the polymer becomes moist and swells (wetting theory). Then, noncovalent (physical) bonds are created within the mucus–polymer interface (electronic and adsorption theory). Then, the polymer and protein chains interpenetrate (diffusion theory) and entangle together to form further non-covalent and covalent bonds (electronic and adsorption theory) [5].

Mucoadhesives are characterized by material properties that contribute to good adhesiveness, according to one or more theories of mucoadhesion. Such material properties are the ability of mucoadhesives to swell, their ability to form molecular (covalent and non-covalent) bonds with the mucus layer, and their spatial conformation due to the entanglement of chains. The creation of molecular bonds and the entanglement of chains lead to changes in the rheological behavior of the mucoadhesives. The rheological properties of mucoadhesives can therefore be used as an indication of the extent of molecular bonding and spatial conformation. The cohesiveness of mucoadhesives contributes indirectly to their adhesive ability, since it concerns the internal strength of the mucoadhesive [5].

The network structure of a hydrophilic matrix will determine its properties as a drug delivery device. There are three main parameters that characterize the hydrophilic matrix network structure:

- The volume fraction in swollen state.
- The molecular weight of the polymer chain between two neighboring crosslinking points.
- The corresponding mesh size.

The polymer volume fraction in swollen state is a measure of the amount of fluid absorbed and retained by the hydrogel. The molecular weight between crosslinks is a measure of the degree of crosslinking of the polymer. The mesh size provides a measure of the distance between consecutive junctions or crosslinks. It offers a measure of the space available between the macromolecular chains for drug diffusion [6].

* Corresponding author. Avda. Joan XXIII s/n, 08028 Barcelona, Spain.
Email address: jaumesauri@hotmail.com (J. Saurí)

http://dx.doi.org/10.1016/j.jddst.2017.03.009
1773-2247/

The aim of this article is to characterize the physicochemical properties and evaluate the potential mucoadhesion capabilities of hydrophilic matrix tablets. Complementary methodologies have been used (cryo-SEM, contact angle and confocal microscopy) to evaluate the potential mucoadhesion capabilities of the formulations. A theoretical description of the mechanisms involved in mucoadhesion has been provided to determine which physicochemical properties are involved in the adhesion process. The pharmaceutical development is described in previous studies [7–10]. Considering that the network structure of a hydrophilic matrix will determine its properties as a drug delivery device [6], an exhaustive analysis of the network structure of the formulations has also been performed.

2. Materials and methods

2.1. Materials

The active substance under study is Captopril (Farmahispania, Spain).

The excipients used for the formulation of tablets were microcrystalline cellulose (Avicel® PH101, FMC Biopolymer (Norway)), barium sulfate (Panreac, Spain), Ascorbic Acid (Fagron, Spain), ethylcellulose (Ethylcellulose N100®, Aqualon, (USA)), and hydroxypropylmethylcellulose (HPMC K15M Premium®, Colorcon, Inc. (USA)). Other ingredients used were talc (Fagron, Spain), magnesium stearate (Fagron, Spain), and colloidal silicon dioxide (Aerosil®, Fagron, (Spain)).

2.2. Methods

2.2.1. Differential scanning calorimetry (DSC) and thermogravimetry analysis (TGA)

DSC analyses (DSC 822e, Mettler Toledo, Switzerland) have been obtained with approximately 5 mg of sample (active ingredient, excipients and binary mixtures). A nitrogen atmosphere with a flow of 50.0 ml min^{-1} and a heat flux of 10 °C min^{-1} in a temperature range of 30.0–300.0 °C was used. The thermograms were analyzed with the help of the Mettler Toledo Star System program, recording the peak positions and quantifying the enthalpy values corresponding to each endotherm. The possible interactions were deduced from the modifications of the thermogram parameters of the mixtures with respect to those seen in the thermograms of pure components.

The thermograms of Captopril, excipients and binary mixtures of Captopril with each of the excipients in the formulation were analyzed with a ratio of 1:1 w/w, which corresponds to the theoretical percentage of the components in the formulation and with a ratio of 1:2 w/w. In the case of ethylcellulose and hydroxypropylmethylcellulose, theoretical percentages of Formulations 1 and 7 were chosen, respectively.

DSC measurements on pure and hydrated hydroxypropylmethylcellulose were carried out with two different calorimeters, a Q100 calorimeter from TA-Instruments operating between 200 K and 450 K, and a liquid-nitrogen DSC 2920 calorimeter allowing measurements as low as 130 K. In both cases, the heating/cooling rate was set to 10 K min^{-1}. Thermogravimetry (TGA) scans were also acquired on the same samples, while heating the sample under N_2 flow between room temperature (300 K) and 400 K at a rate of 2 K min^{-1}, by means of a Q50 thermobalance from TA-Instruments.

2.2.2. Experimental design and manufacturing process

The design of two-components (Formulations 1 to 7) was used in which the variables are the concentration of ethylcellulose N100® and HPMC K15M Premium® by setting all other components of the formula in a 70% w/w, with a 30% w/w maximum concentration for each of the variables. The different formulations are shown in Table 1.

The manufacturing process of the formulations was as follows: the following raw materials were mixed in a container: captopril, ascorbic acid, talc, ethylcellulose N100®, HPMC K15M Premium®, barium sulfate and 70% of the Avicel® PH101. Subsequently the product was mixed for 2 min, it was sieved in a 0.8 mm sieve, it was transferred to a suitable container and mixed for 8 min at 20 rpm in the Glatt biconical mixer. This intermediate product is called mixture A. In another container, 30% of the Avicel® PH101, Aerosil® and the magnesium stearate were mixed for 2 min. The product was sieved in a 0.6 mm sieve and was incorporated to mixture A. Finally, the product was mixed at 20 rpm for 3 min in the biconical Glatt drum.

The blends were compressed in a Bonals® (Cornellà de Llobregat, Spain) continuous eccentric press, provided with 19 × 10 mm punches. The height varied between 6.15 and 6.45 mm, and the weight was 1 g. The formulations comply with the uniformity of mass test (European Pharmacopeia method 2.9.5), since none of the individual masses deviate from the average mass by more than 5%. The average hardness values were between 161 and 195 N (see Table 2).

2.2.3. In vitro dissolution studies

Dissolution was measured with a fully calibrated dissolution apparatus, using the paddle method (Apparatus II, Erweka DT80, Switzerland). The paddle speed was 50 rpm, temperature 37 °C ± 0.5 °C, and volume of the medium 900 ml HCl 0.1 N (pH = 1,2), simulating gastric conditions. At predetermined time intervals, 5 ml samples were withdrawn with replacement. The collected samples were diluted 1:5 with HCl 0.1 N and filtered through the 0.45 μm filters, suitably diluted with the release medium, and ab-

Table 1
Composition of the different formulations (References [1–7]).

Raw materials	Percentage (%)						
	1	2	3	4	5	6	7
Ethylcellulose N100®	30	25	20	15	10	5	0
HPMC K15M Premium®	0	5	10	15	20	25	30
Captopril	10	10	10	10	10	10	10
Talc	4	4	4	4	4	4	4
Aerosil®	0.5	0.5	0.5	0.5	0.5	0.5	0.5
Magnesium stearate	0.5	0.5	0.5	0.5	0.5	0.5	0.5
Avicel® PH101	25	25	25	25	25	25	25
Ascorbic Acid	20	20	20	20	20	20	20
Barium sulphate	10	10	10	10	10	10	10
Total	100	100	100	100	100	100	100

Table 2
Rupture strength values obtained in the different formulations.

	Formulations						
	1	2	3	4	5	6	7
Rupture strength (Newtons)	172 ± 16	169 ± 20	174 ± 25	169 ± 62	161 ± 58	177 ± 30	195 ± 25

sorbance was measured using a UV spectrophotometer (Specord 205 AnalytikJena, Switzerland) at 206 nm and 244 nm to quantify the Captopril and ascorbic acid, respectively. Experiments were performed on all six media.

A multivariate UV-method was used to determine the concentration of Captopril and ascorbic acid in the sample aliquots removed during the dissolution experiment. The calibration model used for prediction was based on UV spectra of 12 calibration samples of known Captopril and ascorbic acid concentrations. The calibration design employed ensured that there was no covariance between the two analytes [10].

The equation of the regression line of captopril relating the concentration to the absorbance corresponds to $Y = 0.037X - 0.005$ at 206 nm. The coefficient of determination is 0.998. The coefficient of variation of the response factor is 3.9% at 206 nm. With the results obtained it is shown that the analytical method is linear in the dissolution test, demonstrating the ability to provide results which are directly proportional to the concentration of captopril.

The average percentage of captopril in the accuracy test is 98.0%, and the coefficient of variation in the precision test is 3.4%. The analytical method developed in order to quantify the captopril in the dissolution test complies with the criteria of specificity, linearity, precision and accuracy in the range between 3 and 25 μg/ml.

The critical quality attribute of major importance is the dissolution rate. Although the absorption of Captopril is independent of concentration and dose [11], its permeability is concentration-dependent [12]. Furthermore, degradation of Captopril is inversely proportional to the concentration of dissolved active substance [12], which is of great importance to obtain a knowledge space to allow selecting a formulation at optimum dissolution rate. The design space was performed based on the percentages of Captopril dissolved at 180, 360 and 600 min.

The values obtained for each formulation designed were processed statistically using Statgraphics Centurion XVI software.

2.2.4. Contact angle measurements and surface free energy determination

The contact angles of water and diiodomethane were determined against tablets of formulations 1, 4 and 7, using the sessile drop method. Results were obtained using a Contact Angle System OCA15plus (Dataphysics, Germany) and were analyzed using SCA20 software (Dataphysics, Germany) in ambient conditions. Using a micro-syringe, a drop of water (2 μl) and diiodomethane (2 μl) were dispensed onto tablet surfaces with a dosing rate of 1 μl/s. The contact angle of the drop was recorded at 0 and 1.2 s using the internal camera, and the contact angles observed during this time period were determined by the software incorporated within the system. Three determinations of each formulation were performed with both solvents. The dispersive and polar surface energy were determined using the angle of the drop recorded at 0 s.

In the method of Wu [13], solid surface free energy can be assessed by the contact angle measurement of two liquids of known polarity and can be assessed by solving one equation with two unknowns (equation (1)).

$$(1+\cos\theta)\,{}_{\gamma}l = 4[({}_{\gamma}{}^{d}s \times {}_{\gamma}{}^{d}l) / ({}_{\gamma}{}^{d}s + {}_{\gamma}{}^{d}l) + ({}_{\gamma}{}^{p}s \times {}_{\gamma}{}^{p}l) / ({}_{\gamma}{}^{p}s + {}_{\gamma}{}^{p}l)] \quad (1)$$

where ${}_{\gamma}l$ is the liquid surface tension and ${}_{\gamma}s$ the solid surface free energy [14]. The solvents commonly used to determine surface free energy are water and diiodomethane (see Table 3).

The spreading coefficients of polymer over mucus, mucus over polymer, and liquid phase over mucus are described in equations (2)–(4).

Table 3
Surface tension of the solvents used for surface free energy determination.

Solvent	γ^{d} (mN/m)	γ^{p} (mN/m)	γ^{TOT} (mN/m)	Work of cohesion
Water	21.8	50.2	72.0	144.0
Diiodomethane	50.4	0	50.4	100.8

$$S_P/2 = -\alpha_P{}^2 - \beta_P{}^2 - (\alpha_M \times \alpha_L) - (\beta_M \times \beta_L) + \alpha_P(\alpha_L + \alpha_M) + \beta_P(\beta_L + \beta_M) \quad (2)$$

$$S_M/2 = -\alpha_M{}^2 - \beta_M{}^2 + (\alpha_M \times \alpha_L) + (\beta_M \times \beta_L) - \alpha_P(\alpha_L - \alpha_M) - \beta_P(\beta_L - \beta_M) \quad (3)$$

$$-S_L/2 = \alpha_L{}^2 + \beta_L{}^2 - (\alpha_M \times \alpha_L) - (\beta_M \times \beta_L) - \alpha_P(\alpha_L - \alpha_M) - \beta_P(\beta_L - \beta_M) \quad (4)$$

where α_P and β_P are the polar and dispersion forces of the polymer, α_M and β_M are the polar and dispersion forces of the mucus, and α_L and β_L are the polar and dispersion forces of the gastrointestinal fluid. The values for the polar and dispersion components of mucus (pig intestinal mucosa in isotonic saline: $\alpha = [3.52\ mN/m]^{0.5}$, $\beta = [5.26\ mN/m]^{0.5}$), and gastrointestinal fluids (taken as water for which the values of $\alpha = [4.67\ mN/m]^{0.5}$ and $\beta = [7.14\ mN/m]^{0.5}$ are considered standard) [15].

The combined spreading coefficient (S_c) for mucoadhesion is described in equation (5):

$$S_C = (-S_L/2)^{0.5} \times (S_P/2)^{0.5} \quad (5)$$

where $(-S_L/2)^{0.5}$ is the Griffith fracture energy (${}_{YG}{}^{0.5}$).

Bioadhesion can be modeled by use of surface energetics and spreading coefficients [15]. It is necessary to view the spreading coefficient in relation to three phases, namely the drug delivery system, the mucus layer and the gastrointestinal fluid, where the fluid is displaced from the mucus surface by the polymeric delivery system. Consequently, three spreading coefficients exist, one for the polymer over mucus (S_P), one for mucus over polymer (S_M), and the other for the gastrointestinal liquid over the mucus (S_L). The requirement for mucoadhesion is that the spreading coefficient for the gastrointestinal liquid over the mucus (in the presence of the polymer) is negative (disfavored). The negative value for S_L is a requirement, but not a sufficient condition, for mucoadhesion. It is also necessary for one of the other spreading coefficients to be positive (favored) to provide spontaneous and stable adhesion. This double requirement is a consequence of the three-phase competitive interaction [16].

Spreading of the mucosal phase is not likely if the adhesive polymer is a hydrogel. Therefore, the mucosa-spreading coefficient (S_M) will always be negative, but can be neglected if $S_P > 0$.

2.2.5. Confocal microscopy

The morphology and surface roughness of the tablets were characterized after adding 2 ml of water in formulations 1, 4 and 7.

The surface texture was measured with a Confocal Leica 3DCM microscope with an EPL 20x/0.50 objective, covering an area of 636.61 μm × 477.25 μm. Eight quantitative parameters were used to characterize the morphology and roughness of the tablet surface of formulations 1, 4 and 7: arithmetic mean deviation of the surface (Sa), root-mean-square deviation of the surface (Sq), skewness of the topography height distribution (Ssk), kurtosis of the topography height distribution (Sku), 10-point mean of the absolute heights (Sz), height of highest peak (Sp), depth of deepest valley (Sv), and vertical distance between the highest peak and deepest valley (St).

Millimeter scale areas of the tablet surfaces were measured using a confocal microscope (LEICA DCM3D, Leica Microsystems, Germany), which was used to image and measure the roughness of the tablet surfaces. The measurement Z-range was ±50 μm and the resolution was 500 nm (lateral) and 30 nm (vertical) using image sizes of 0.6 mm × 0.43 mm. Confocal microscopy provides the distribution of surface peaks and valleys without the need for complex sample preparation.

2.2.6. Scanning electron microscopy

To observe the amorphous structure of the gel layer, the tablets were placed in a 400 ml glass beaker with water in a magnetic stirrer for 5 s at 300 rpm. Hydrated tablet samples were examined by the Cryo-SEM method by means of a cryostage (GATAN ALTO-1000, USA) attached to the scanning electron microscopy (SEM JEOL JSM-6510, Japan), which can maintain the structure of the hydrated materials in the most natural state. Hydrated samples were frozen by plunging them into liquid nitrogen, and then transferred in vacuum to the cryo-unit system coupled with the SEM. Samples were sublimated at −70 °C for 15 s in the SEM chamber in high vacuum conditions. Then, the tablets were relocated in the cryo-unit in order to be sputtered with gold. The covered samples were finally observed in the SEM at 10 kV maintaining the temperature at −192 °C. The images were taken using the tablets of formulations 1, 4 and 7.

2.2.7. Dielectric spectroscopy study of molecular dynamics of HPMC K15M

To study the interaction of hydroxypropylmethylcellulose (HPMC K15M) with water and the resulting molecular dynamics, we carried out a comparative study on three different forms of HPMC: powder, aqueous solution, and as hydrated thin film. To obtain the aqueous solutions, HPMC K15M was mixed with pure deionized water in a 2% weight-volume ratio and sonicated for a few minutes to ensure homogeneity. A rather viscous liquid was obtained. Thin hydrated films were obtained by slow (ambient temperature) evaporation of the solution in a glass beaker. All three types of samples were characterized by DSC and broadband dielectric spectroscopy (BDS). The powder and the hydrated films were also characterized by TGA to determine their water content.

For BDS measurements, different capacitor cells were used for each type of sample. To obtain pellets, the powder was mechanically pressed between two steel disks, used as capacitor plates. The films were recovered between the same two disks. As for the aqueous solutions, the samples were inserted at room temperature in liquid form inside a home-made stainless steel parallel-plate capacitor, specially designed for liquid samples, with the two cylindrical plates separated by needle-like silica spacers of 50 μm in diameter. The capacitors were then loaded into a nitrogen-gas flow cryostat for temperature control. Dielectric spectra were acquired in the frequency (f) range from 10^{-1} to $5{\cdot}10^{6}$ Hz using a Novocontrol Alpha analyzer. Experiments were carried out in the temperature range between 500 and 120 K.

Dielectric spectroscopy yields the complex permittivity of a sample as a function of frequency. In dielectric measurements, an AC electric field is applied to a parallel-plate capacitor formed by a homogeneous sample between two metal disks. Using the known surface area and the thickness of the dielectric sample, the complex permittivity is directly extracted from the complex impedance of the capacitor cell, which is measured with an impedance analyzer. This technique allows probing in the same experiment both the AC conductivity and the molecular dipolar dynamics. In this study, the dielectric spectra are displayed either as dielectric loss (imaginary permittivity, $\varepsilon''(f)$) or as AC conductivity $\sigma'(f)$). The two representations are related by $\sigma'(f) = 2\pi f\, \varepsilon_0\, \varepsilon''(f)$. In the temperature range under study, all samples displayed one or two losses. The data could be fitted assuming that each loss was described by a Cole-Cole or Debye function, to which a background was sometimes added representing the DC conductivity contribution, following the usual fitting procedure for BDS spectra. For temperatures below 260 K, each AC conductivity spectrum and corresponding loss spectrum of these samples was fitted as the sum of two relaxation processes, modeled one with a Cole-Cole function and the other a Debye function. The analytic expression of the complex Cole-Cole function is described in equation (6) [17]:

$$\varepsilon_{CC}(f) = \varepsilon_{\infty} + (\Delta\varepsilon/1) + \left(f/f_{\max}\right)^{c} \tag{6}$$

Here $\Delta\varepsilon = \varepsilon_s - \varepsilon_\infty$ is the dielectric strength, ε_∞ and ε_s are the high-frequency and static low-frequency limits of the real permittivity. The parameter c, called the Cole–Cole exponent, lies in the range from 0 to 1 and is related to the width of relaxation time distribution; finally, f_{max} is the frequency at which the dielectric loss of the given relaxation process is highest. The Cole-Cole function is a phenomenological modification of the Debye law [18], which is described in equation (7):

$$\varepsilon_{Debye}(f) = \varepsilon_{\infty} + (\Delta\varepsilon/1) + \left(f/f_{\max}\right)^{c} \tag{7}$$

which corresponds to Eq. (6) with $c = 1$. The characteristic frequencies f_{max} vary exponentially with temperature and are therefore usually plotted in the Arrhenius representation (Log(f_{max}) *vs* 1/T). The same holds for the DC-limiting value of conductivity, σ_{dc}, defined as the plateau value in a $\sigma'(f)$ spectrum.

3. Results and discussion

3.1. Differential scanning calorimetry (DSC) analysis

Table 4 sets out the temperatures and melting enthalpies for each of the samples tested.

The Captopril DSC curve shows an endotherm between 104 and 113 °C ($\Delta H_{melting} = -121$ J g^{-1}), with a melting temperature of 107.3 °C (T_{onset}) and 109.5 °C (T_{peak}).

Captopril presents incompatibility with magnesium stearate [19]. However, this incompatibility depends on the ratio of the components (see Table 4). One possible explanation is that magnesium stearate increases the pH of the microenvironment of the formulation due to its basicity, which will interact with Captopril, since it is unstable at basic pH. However, if an amount of magnesium stearate that does not modify the pH of the microenvironment of the formulation is added to the formulation, there is no incompatibility between the two components. With the ratio 1:1 w/w there is no incompatibility between

Table 4
Thermoanalytical data of Captopril and drug:excipient physical mixtures.

Samples	DSC				Enthalpy (melting) J g-1	
	T onset (melting)/°C		*T* peak (melting)/°C			
Drug						
Captopril	107.3	109.5	−121			
Drug/excipient	1:1	1:2	1:1	1:2	1:1	1:2
Microcrystalline cellulose PH101	106.1	104.5	108.8	108.3	−31	−29
Ethylcellulose N100	106.7	105.7	108.5	108.2	−12	−9
Hydroxypropylmethylcellulose K15M	106.5	105.2	108.9	108.6	−25	−17
Ascorbic acid	105.0	104.4	108.5	108.1	−39	−24
Talc	107.2	106.0	109.4	109.4	−86	−74
Barium Sulfate	106.1	106.2	109.6	109.3	−59	−48
Magnesium stearate	102.2	97.4	107.2	106.7	−100	−84
Colloidal silicon dioxide	105.9	106.2	110.2	109.5	−114	−110

the two components, while with the binary mixture 1:2 w/w, the melting temperature of Captopril (Tonset) is 97.4 °C, which may suggest a possible incompatibility between magnesium stearate and Captopril.

The DSC of the mixtures with the other excipients of the formulation obtained can be considered a superposition of the individual profiles, highlighting the absence of incompatibilities between Captopril and excipients.

3.2. Dissolution profiles

Fig. 1 shows the Captopril release profiles from the HPMC matrices where there is a significant change in the release profiles between 5% and 10% w/w of HPMC K15M. Above 10% w/w of HPMC K15M (the polymer percolation threshold), an infinite cluster of this component is formed which is able to control the hydration and release rate [20]. Above 25% w/w of HPMC K15M, the release rate does not decrease, which is normal in formulations of drugs that are highly soluble in water [21].

The burst release effect is more predominant when the percentage of ethylcellulose N100 is increased with respect to HPMC K15M. The dissolution rate of Captopril is inversely proportional to the concentration of HPMC K15M. Formulation 4 has the optimum modified release profile, since formulations 5, 6 and 7 show a retention of Captopril in the matrix that does not permit the release of Captopril in the dissolution test.

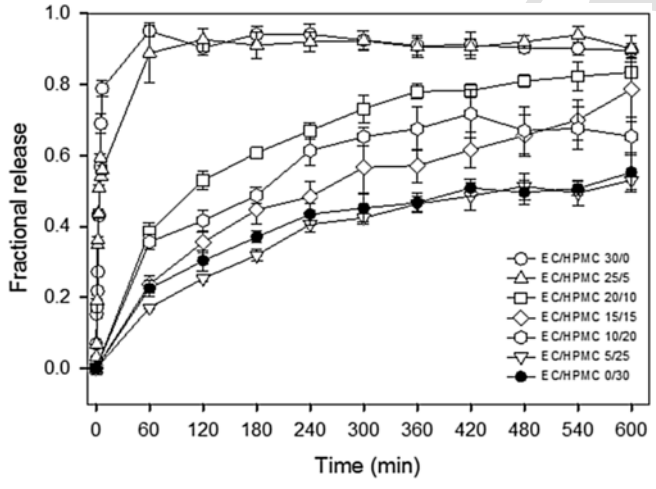

Fig. 1. Dissolution profiles of the different formulations (1–7) in HCl 0.1 N (pH = 1.2) at 37 °C, and paddle speed at 50 rpm.

3.3. Design space

Fig. 2 shows the models best suited to the data obtained from the dissolution profiles. At 180 min, the model that best fits is the square-root X:Y model, while at 360 and 600 min, the model that best fits is the linear model.

Analysis of variance (ANOVA) was used to study the validity of the model. Since the p-values in the ANOVA table are below 0.01 (see Table 5), there is a statistically significant relationship between the percentage of Captopril dissolved at 180, 360 and 600 min with the formulations for a confidence level of 99%. This indicates that the three models are valid for relating the variation of responses to the variation of the factors, which allows describing the design space. At 180 min, there is an interaction between the ethylcellulose and HPMC K15M in the dissolution rate of Captopril. The interaction between the components disappears with time and the model becomes linear and is more linear at 600 min than at 360 min (see Fig. 2).

3.4. Physicochemical characterization of hydrophilic matrix tablets

3.4.1. Wetting properties

The hydration process is essential for the relaxation and interpenetration of polymer chains. Controlling the rate and extent of hydration is required to produce prolonged adhesion. When the concentration of ethylcellulose N100 increases, the contact angle decreases and, in consequence, the surface free energy and the wettability of the tablets increases (see Tables 6 and 7).

Secondary hydrogen and Van der Waals bonds contribute to the swelling ability of polymers, which favors the presence of rheological synergism and leads to improved mucoadhesion. This spreading process, controlled by the interfacial energies of the mucus and the drug delivery system, allows close contact at the mucus–drug delivery system interface, thus governing the formation of bonds [15].

When the concentration of ethylcellulose N100 increases, the polar and the dispersion forces increase (see Table 7). The values of the spreading coefficients of polymer over mucus and the spreading coefficients of mucus over polymer are negative, which is why these processes are not spontaneous. However, these processes are more favored when the concentration of HPMC K15M is increased. Although the values of the spreading coefficients are negative, the extension of polymer over mucus will be predominant with respect to the extension of the mucus over the polymer, since the values of the spreading coefficients of polymer over mucus are less negative than the values of spreading coefficients of mucus over polymer. The extension process of the mucus over polymer cannot be neglected because the values of the spreading coefficients of the polymer over mucus are not positive (see Fig. 3). The combined spreading coefficient has not been calculated because the values of the spreading coefficients of polymer over mucus are negative. For this reason, all the spreading coefficients (S_P, S_M and S_L) have to be taken into account to predict the bioadhesion of the formulations. All values of spreading coefficients of liquid phase over mucus are negative, indicating that this process is not spontaneous. However, when the concentration of HPMC K15M increases, the liquid phase tends to spread less in the mucus layer (see Fig. 3), and the spreading coefficients of polymer over mucus and mucus over polymer are more positive. Therefore, the contact between the matrix tablets with the mucus layer will be increased.

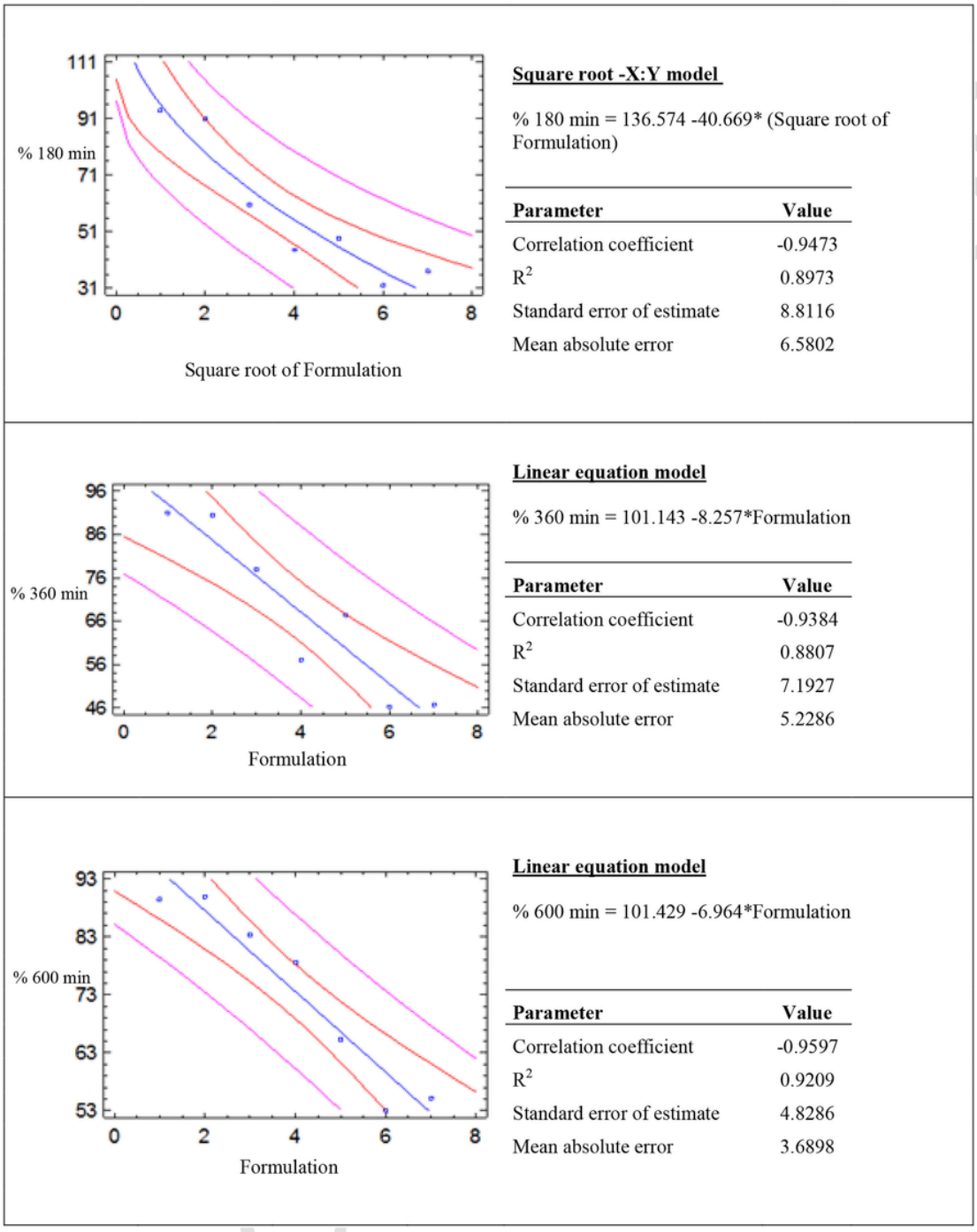

Fig. 2. Equations of the models at 180, 360 and 600 min. The X axis corresponds to formulations, while the Y axis corresponds to % Captopril dissolved.

Rough surfaces also provide an increased surface area available for interaction along with enhanced viscoelastic and plastic dissipation of energy during joint failure, which are thought to be more important in the adhesion process than a mechanical effect. Table 8 shows the parameters of surface texture analysis of formulations 1, 4 and 7, after wetting. Formulation 4 presents the highest value of Sq (root mean square of height). The Sdar/Spar ratio is shown in Table 8, where Sdar is the total developed area of a rough surface, and Spar is the projected area: 303,822 μm^2 = 636.61 × 477.25 μm^2. This ratio represents the value of developed area per unit of projected area and is connected with the volume of the surface roughness (volume of peaks and valleys). The developed area ranges from around 112 times the projected area for formulation 1 to 1508 times for formulation 4. After water uptake, all parameters show a greater swelling surface in formulation 4 than in the other two formulations. Formulation 4 presents a greater swelling capacity and a greater increase in surface roughness (see Table 8), therefore there is more available surface to establish physicochemical interactions with the mucus layer.

Table 5
ANOVA summary (dissolution test).

Source of variation	Sum of squares	Degrees of freedom	Mean Squares	F-Ratio	*P*-Value
X:Y square root model for % response Captopril dissolved at 180 min.					
Model	3391.81	1	3391.81	43.68	0.0012*
Residuals	388.222	5	77.6445		
Total	3780.03	6			
Linear model for % response Captopril dissolved at 360 min.					
Model	1909.05	1	1909.05	36.90	0.0017*
Residuals	258.677	5	51.7354		
Total	2167.73	6			
Linear model for % response Captopril dissolved at 600 min.					
Model	1358.04	1	1358.04	58.25	0.0006*
Residuals	116.579	5	23.3157		
Total	1474.61	6			

*p-value <0.01 indicates significance level.

Table 6
Contact angle of water and diiodomethane with formulations 1, 4 and 7.

Water	Advancing contact angle (θ_A)	Receding contact angle (θ_R)	Contact angle Hysteresis
Formulation 1	34°± 2	0°± 0	34°
Formulation 4	38°± 5	0°± 0	38°
Formulation 7	39°± 3	20°± 23	19°
Diiodomethane	Advancing Contact angle (θ_A)	Receding Contact angle (θ_R)	Contact angle Hysteresis
Formulation 1	31°± 5	0°± 0	31°
Formulation 4	31°± 3	0°± 0	31°
Formulation 7	36°± 1	0°± 0	36°

Table 7
Surface free energy of formulations 1, 4 and 7.

	Y^p (mN/m)	Y^d (mN/m)	Y^{TOT} (mN/m)
Formulation 1	29.0	43.9	72.9
Formulation 4	27.1	44.1	71.2
Formulation 7	27.3	41.7	69.0

3.4.2. Network structure of the hydrophilic matrix tablets

Although many factors are involved in such processes, the fundamental properties that significantly influence this inter-movement are cross-linking density, molecular weight, chain mobility/flexibility and expansion capacity of both networks [2].

High cross-linking restricts mucoadhesive ability by decreasing the amount of free macromolecular chains able to diffuse in the mucus layer [5]. The degree of cross-linking within a polymer system significantly influences chain mobility and resistance to dissolution. As cross-link density increases, chain mobility decreases and hence the effective chain length which can penetrate into the mucus layer decreases, reducing mucoadhesive strength [2].

When the concentration of HPMC K15M increases, the cross-linking density increases (see Fig. 4). The porosity of formulation 1 is produced by the dissolution of the components as it has no HPMC K15M in the formulation, which is why tablet integrity decreases due to not having crosslinks that enable tablet strength in the aqueous medium. The porosity of formulations 4 and 7 is generated by the crosslinking between the HPMC K15M chains. When the concentration of HPMC K15M increases, pore size decreases (see Fig. 4). The integrity of the tablet decreases by increasing the percentage of the ethylcellulose N100 in the formulation [8].

With the results obtained and taking into account that as the concentration of HPMC K15M increases, the degree of crosslinking increases, formulation 4 has a greater mucoadhesive ability compared to formulation 7, since the availability of HPMC K15M chains for diffusion in the mucus layer is greater. Furthermore, due to the larger pore size, mucin glycoproteins can penetrate the matrix tablets more easily, favoring the physicochemical interactions of the components of mucus with the components of the hydrophilic matrix, thus increasing the mucoadhesion of the formulation.

3.5. Thermophysical characterization and dielectric spectroscopy of HPMC K15M

Chain flexibility is critical for interpenetration and entanglement with the mucus. Increased chain mobility leads to increased inter-diffusion and interpenetration of the polymer within the mucus network

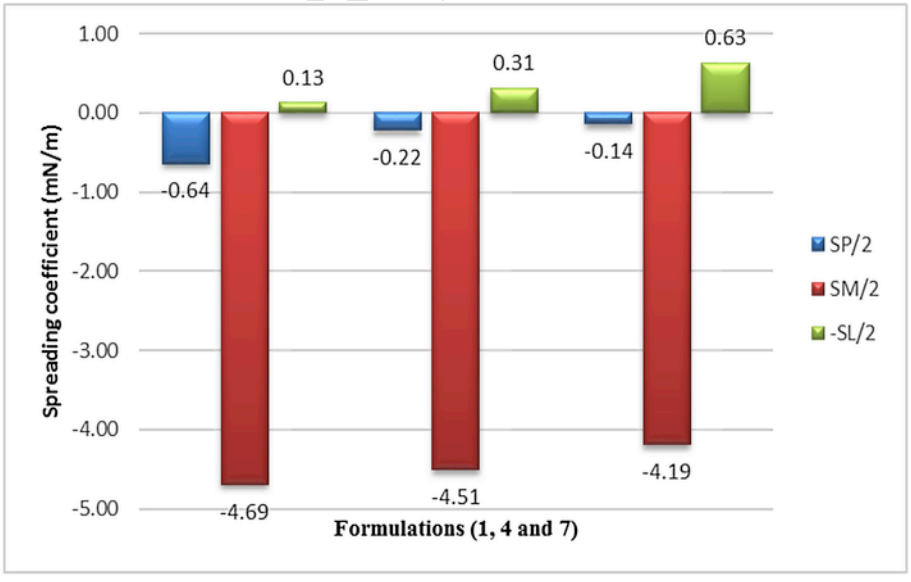

Fig. 3. Spreading coefficients of the formulations 1, 4 and 7.

Table 8
Surface texture parameters of formulations 1, 4 and 7, after wetting.

Parameter	Formulation 1	Formulation 4	Formulation 7
	Amplitude Parameters		
Sa	14.798	46.360	24.821
Sq	23.464	68.668	38.821
Sz	240.265	548.164	307.768
Sp	112.393	266.356	169.584
Sv	141.941	303.511	142.300
St	254.335	569.867	311.884
Ssk	−1.496	−0.748	0.504
Sku	8.653	5.477	5.953
	Other parameters 3D		
Sdar	34,282,010	458,196,407	171,963,409
Spar	303,822	303,822	303,822
Sdar/Spar	112.8	1508.1	566.0

[2]. In view of this, we have employed broadband dielectric spectroscopy (BDS) to characterize the chain flexibility/mobility of pure and hydrated hydroxypropylmethylcellulose (HPMC K15M), the excipient that has the adhesive properties. We have only considered HPMC K15M and an aqueous mixture thereof due to the intrinsic difficulty of considering ternary mixtures (hydroxypropylmethylcellulose, ethylcellulose and water), and because HPMC K15M in contact with water forms the gel layer responsible forthe adhesiveness of the tablet. The totally different aqueous behavior of ethylcellulose and HPMC K15M can be observed in the right-hand panels of Fig. 4: the samples containing HPMC K15M display a formation of structures with smooth boundaries and interconnected by polymer filaments (formulations 4 and 7); such structures are completely absent from formulation 1, which exhibits pointed, rough surfaces with no signs of filamentation.

The glass transition temperature of the HPMC K15M powder (see inset to Fig. 5(a)) was measured by DSC as being $T_g \approx 445$ K, in agreement with previous studies on hydroxypropylmethylcellulose [22,23]. The TGA thermogram of the polymer (Fig. 5(a)) shows a mass loss between 320 and 380 K, peaking at 350 K, the typical desorption temperature of physisorbed water. The glass transition temperature marks the freezing of the cooperative segmental dynamics of the polymer chains. Such dynamics, usually called primary or α relaxation dynamics, are readily detected by BDS in dipolar samples, including many polymers [18] and hydrated samples [24]. The dielectric spectra of the HPMC K15M powder did not show any loss feature above T_g, which indicates that the dipole moment per unit volume of the polymer is too low to be detected by the technique. However, a relatively weak loss feature is observed at and below room temperature. This dielectric feature is related to the presence of physisorbed water, and in fact it disappears upon heating to 400 K.

Very similar behavior was observed for thin HPMC K15M films obtained by slow evaporation of the solution. As can be seen in Fig. 5(b), the relative water content is higher in the films than in the powder. The dielectric loss spectra of a particular thin film sample are shown in Fig. 6(a). A main dielectric loss is visible, accompanied by a weaker feature at higher temperature. Both features shift to higher frequency with increasing temperature, as expected. The low frequency background visible in the spectra acquired at a temperature of 253 K or higher is due to electrical conduction in the film. The dielectric strength of room temperature relaxation in the film is higher than that in the powder, as may be expected due to the lower water content in the latter. Also, in this case relaxation is lost upon heating to 400 K, i.e., when all water is desorbed.

The loss spectra of the 2% aqueous solution, shown in Fig. 6(b), are considerably different from those of the films and powder. Above 0 °C, the spectral lineshape appears dominated by ionic conduction phenomena in the solution, which usually hinders the observation of dipolar relaxations [25]. DSC characterization of the same sample showed that the solution underwent at least partial crystallization just below the freezing temperature of pure water (the melting across this temperature is shown in the inset to Fig. 6). This phenomenon can be seen by the dramatic change in lineshape between the temperatures of 267 and 263 K in Fig. 6(b). Below this temperature, the spectra exhibit two clearly resolved loss features.

To determine the origin of the two loss features observed in the partially crystallized solution, we analyzed the AC conductivity spectra (Log(σ′) *vs* Log(*f*)) of the same 2% sample, plotted in Fig. 7(a).

As can be seen in the Figure, the conductivity spectra above 265 K are indeed dominated by the DC conductivity of the sample, shown as a straight plateau at high frequency. In these spectra the bending at lower frequencies corresponds to a space-charge effect, i.e., to the accumulation of charges (ions) at the sample's heterogeneities (boundaries between amorphous and crystalline domains), which results in lower conductivity. The partial crystallization at approximately 265 K is accompanied by a reduction of the DC conductivity by two orders of magnitude. The spectra below 265 K are more structured than those above: the high-frequency region displays a plateau corresponding to the DC conductivity, but the spectral region of the electrode polarization effect is seen to contain an additional feature. The two bump-like features that can be observed in the AC conductivity spectra below 265 K correspond to the two features visible in the permittivity (loss) representation in Fig. 6(b).

The spectra of Figs. 6(b) and 7(a) were fitted as the sum of two separate components plus a conductivity background. The higher-frequency loss, visible as a shoulder to the main peak in Fig. 7(a), can be unambiguously assigned to the electrode-polarization effect, while the lower-frequency loss (main peak) is ascribed to an intrinsic dipolar loss of the sample. Indeed, the decrease in AC conductivity exactly matches the maximum of the higher frequency loss, and, in turn, such loss could be modeled with a Debye function, as it is typical for space-charge losses [18]. Moreover, in Fig. 7(b) we compare the temperature dependence of the characteristic frequency f_{max} for both losses with that of the DC conductivity σ_{dc} (plateau value of the $\sigma'(f)$ spectra at high frequency). The Arrhenius plot of σ_{dc}, at least below 220 K, displays the characteristic negative curvature, typical of disordered ionic conductors [26,27]. It is observed that, at least at low temperature (below approximately 200 K, corresponding to 1000/T = 5 K^{-1}), where the dipolar relaxation and the conductivity relaxation are clearly separated, the slopes of the Arrhenius plots (effective activation energies) of both σ_{dc} and of f_{max} for the faster relaxation are virtually identical, signaling a common origin of both and thus corroborating the assignment of this feature as a conductivity-related (space-charge) loss [28,29].

The lower-frequency loss is a true dipolar loss, and it had to be modeled with a Cole-Cole function (Eq. (6)). The observation of clear dipolar relaxation indicates that crystallization near 0 °C is only partial, that is, it leads to the formation of crystalline (ice) domains amidst an amorphous polymeric matrix. Conversely, regions where the concentration of water is lower do not crystallize. These amorphous regions are responsible for the dipolar loss observed. Since the polymer does not have a sufficiently large dipole moment for detection by BDS, such dipolar feature involves the motion of water molecules. However, since the solution is initially homogeneous prior to crystallization, the amorphous domains that do not crystallize must retain a significant degree of mixing of polymer chains and water molecules; in other words, the observed dipolar dynamics must corre-

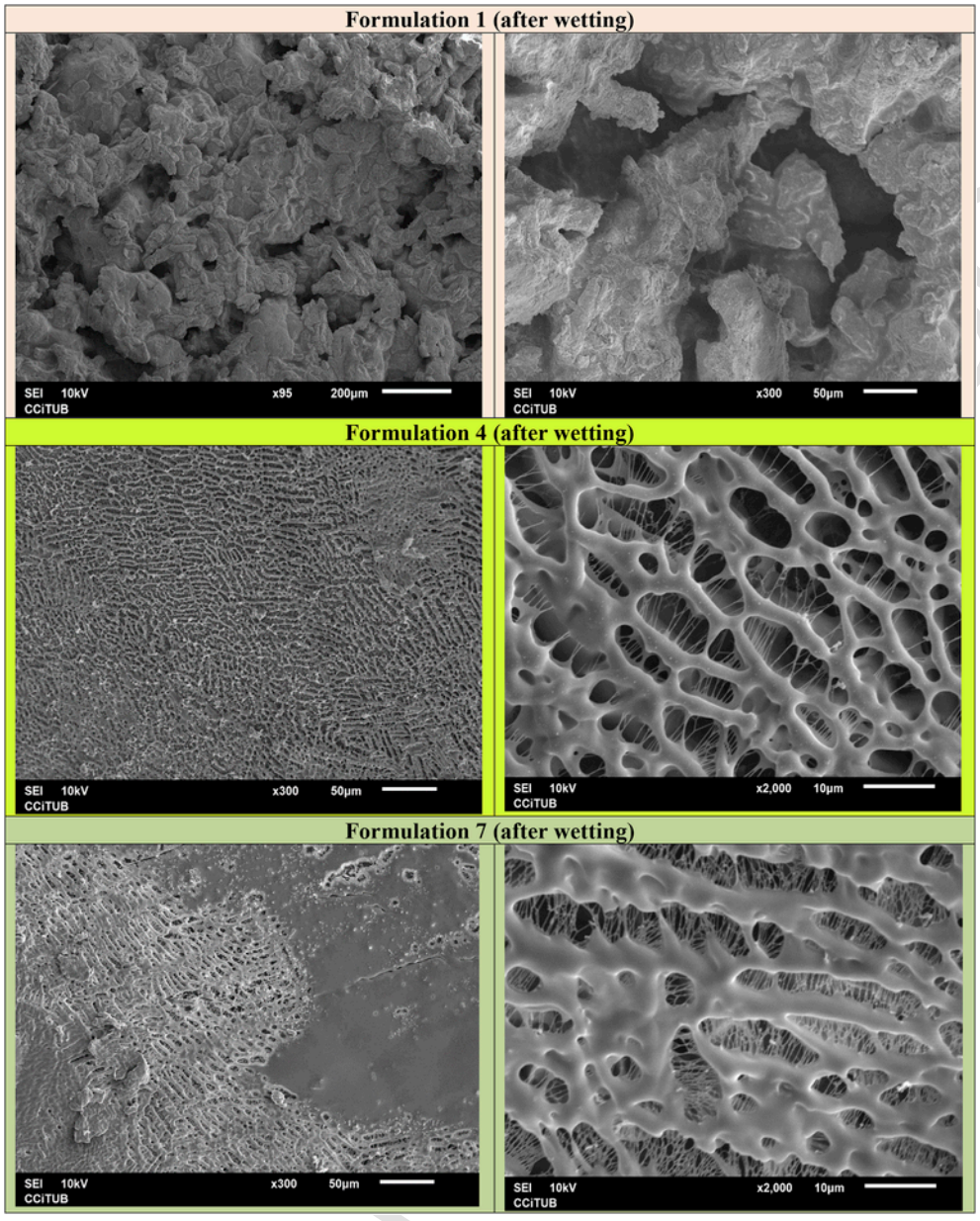

Fig. 4. Morphology of the tablets of formulations 1, 4 and 7 moistened with water. The images were examined by Scanning Electron Microscopy (SEM).

spond to a collective relaxation motion of water molecules linked to cellulose chains.

To confirm that the dipolar relaxation of Fig. 6(b) at least partially also reflects the mobility of the polymer chains, Fig. 8 shows the Arrhenius plot of the characteristic relaxation times of the main (dipolar) loss in all three samples studied (quasi-pure polymer, hydrated film, partially amorphous polymer-water mixture).

It may be observed that, while the frequencies of the water-induced loss in the powder and thin film samples are almost overlapping and have an identical slope (effective activation energy), depending on the temperature the characteristic frequency of the dipolar relaxation in the aqueous mixture can be one order of magnitude smaller or larger than the latter two (as also discernible directly from Fig. 6), and moreover it displays a totally different activation energy. This is a clear indication that while the main losses in the film and in the powder are due to physisorbed water molecules whose reorientational motions are basically independent of the polymer, in the aqueous mixture the water-induced relaxations are strongly influenced by the presence of the polymer chains. Indeed, this observation confirms the idea that the relaxation in the partially amorphous mixtures is a truly collective (water + polymer) relaxation.

The temperature behavior of the dipolar loss of the aqueous mixture could be modeled using a Vogel-Fulcher-Tammann (VFT) dependence, which is described in equation (8) [18]:

$$f_{max} = f_0 \exp\left[-s\, T_{VF}/\left(T - T_{VF}\right)\right] \tag{8}$$

Here the prefactor f_0, the strength parameter s and the so-called Vogel-Fulcher temperature T_{VF} are phenomenological parameters. The fit is shown along with the experimental data in Fig. 8(a). Using this fit it is possible to extrapolate the curve down to the freezing

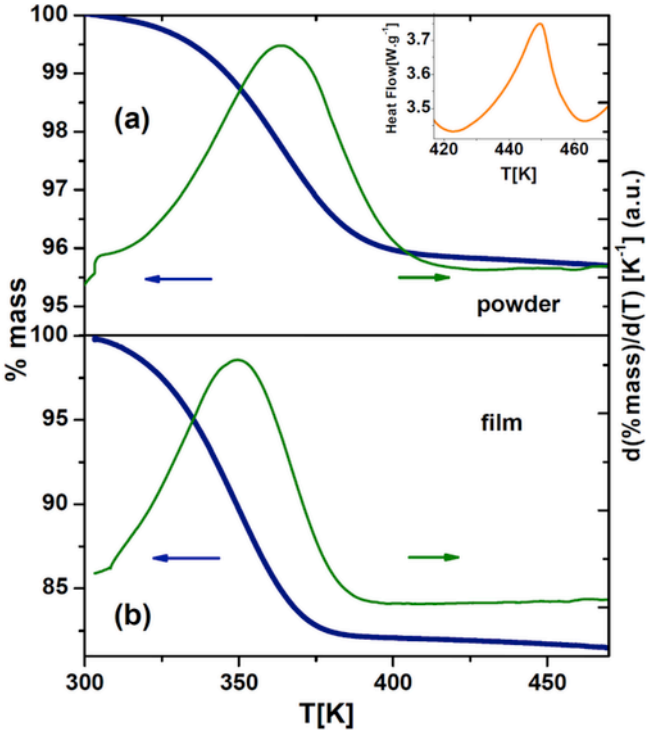

Fig. 5. Thermogravimetry curve (thick line) and derivative thermogram (thin line) of the HPMC K15M powder (a) and of a hydrated HPMC K15M film (b). Measurements are carried out by heating at 2 K per minute. Both samples exhibit a mass loss peaking at 350 K due to desorption of physisorbed water. Inset to (a): Differential scanning calorimetry thermogram of the HPMC K15M powder, measured by heating at a rate of 10 K per minute. A glass transition is observed at approximately 445 K.

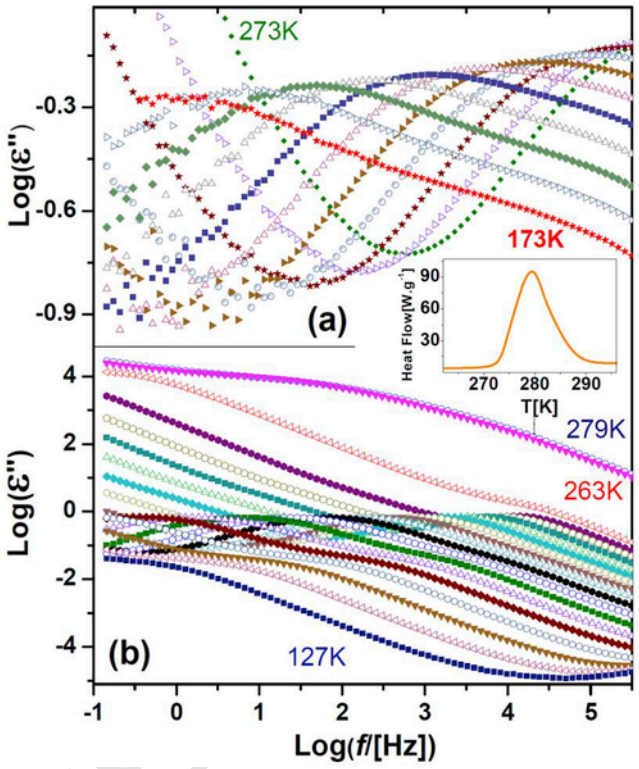

Fig. 6. (a). Isothermal dielectric loss spectra (imaginary permittivity, ε) of the same (hydrated) HPMC K15M film as in Fig. 6(b). Spectra are shown only at selected temperatures (every 10 K) for greater clarity. (b) Analogous spectra of the 2% solution, every 8 K. Inset: Differential scanning calorimetry thermogram acquired upon heating at 10 K per minute the 2% solution, showing (partial) melting above 273 K (0° C).

temperature for this molecular dynamic process, defined as the temperature at which the characteristic motion time reaches 100 s, or equivalently $f_{max} = 10^{-2}/2\pi$ Hz $\approx 1.59 \times 10^{-3}$ Hz. The extrapolated freezing temperature is roughly 140 K. This temperature is found to be close to (though slighly lower than) the temperature of the anomaly observed with low-temperature DSC on the same sample, as reported in the inset to Fig. 8 (roughly 160 K; the anomaly is more visible upon cooling than heating). The fact that the freezing temperature of the dipolar process coincides with a calorimetry anomaly confirms that such process has a molecular dynamic origin, and corresponds in fact to dipolar dynamics in the amorphous (non-crystallized) part of the sample.

To summarize, we assign the slower relaxation feature to the coupled molecular motions of water and the hydrated cellulose chains. The freezing temperature obtained, 165 K, can be taken to be the approximate freezing temperature of local motions in the polymer-water gel. The high mobility of the HPMC K15M chains is an effect of the swelling, which effectively disentangles the chains, and of the interaction with the liquid-like aqueous matrix.

4. Conclusions

It has been demonstrated that the combination of equations based on the wettability, the surface free energy, the swelling of the tablets, and the diffusion of the HPMC K15M chains, along with the microscopic characterization of the hydrophilic matrix, allows us to obtain scientific knowledge that enables characterizing the variables that have an impact in the mucoadhesion process. Considering the tablet surface free energy and the spreading coefficients, when the concentration of HPMC K15M increases, adhesion to the mucus layer will be increased, as the contact between the tablet surface and the mucosa is favored. Formulation 4 is the one that presents greater swelling, a greater increase in surface roughness, and larger pores within the matrix. These results show that formulation 4 has a higher chain mobility, more free macromolecular chains able to diffuse in the mucus layer, and more contact between the tablet surface and the mucosa, and therefore this formulation has the greatest potential mucoadhesion capability. The dielectric spectroscopy study reveals that when mixed with water, HPMC K15M exhibits joint molecular relaxation motions with water molecules. Such motions are observed below the freezing point of water but are obviously also present at room temperature, i.e., far below the glass transition temperature of pure HPMC K15M (172 °C). We assign the relaxation motions to fully hydrated HPMC K15M chains, which are responsible for the adhesive properties of the polymer.

Acknowledgements

This work was partially supported by the Spanish Ministry of Science and Innovation through project FIS2014-54734-P and by the Generalitat de Catalunya under project 2014 SGR-581.

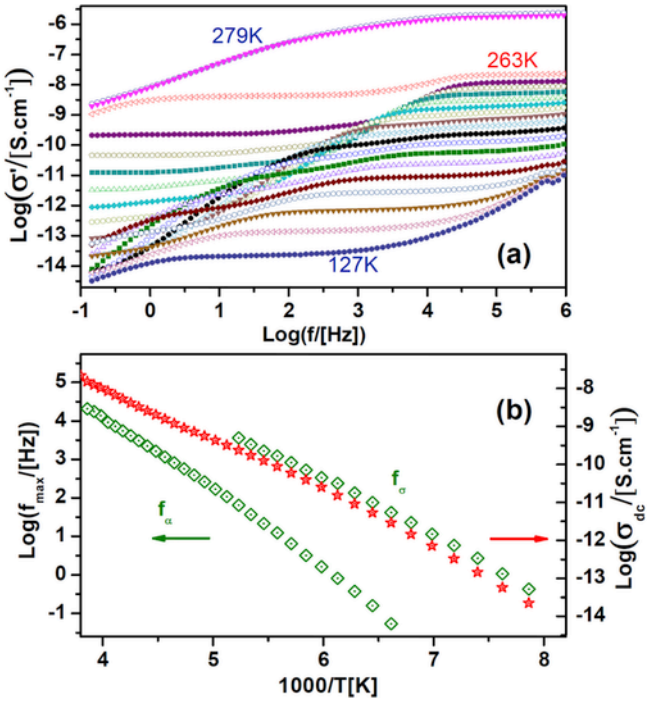

Fig. 7. (a). Alternating-current (AC) conductivity spectra (σ′) of the partially crystallized 2% mass/volume sample, every 4 K. 7(b) Comparison between the characteristic times and the direct-current (DC) conductivity (σ_{DC}) (both vertical scales span the same number of decades).

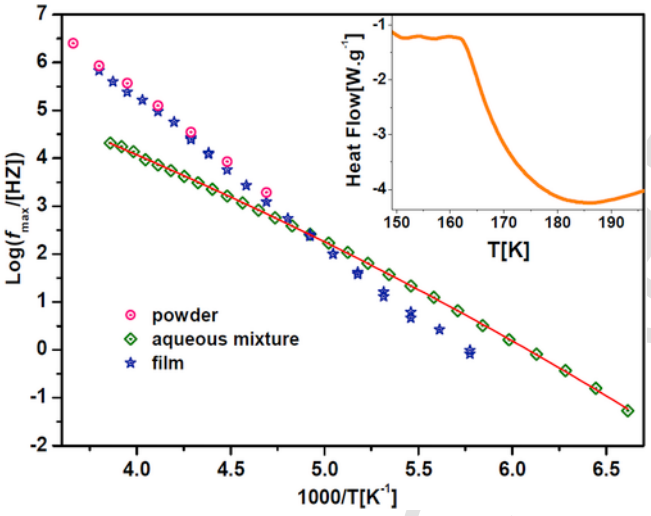

Fig. 8. Arrhenius plot of the characteristic frequencies f_{max} of the most prominent loss in all three forms of HPMC K15M studied (powder, film, aqueous mixture). Inset: low-temperature differential scanning calorimetry thermogram of the 2% mass/volume sample.

References

[1] K. Netsomboon, A. Bernkop-Schnürch, Mucoadhesive vs. mucopenetrating particulate drug delivery, Eur. J. Pharm. Biopharm 98 (2016) 76–89.

[2] G.P. Andrews, T.P. Laverty, D.S. Jones, Mucoadhesive polymeric platforms for controlled drug delivery, Eur. J. Pharm. Biopharm 71 (2009) 505–518.

[3] J.W. Lee, J.H. Park, J.R. Robinson, Bioadhesive-based dosage forms: the next generation, J. Pharm. Sci. 89 (2000) 850–866.

[4] D. Solomonidou, K. Cremer, M. Krumme, J. Kreuter, Effect of carbomer concentration and degree of neutralization on the mucoadhesive properties of polymer films, J. Biomater. Sci. Polym. Ed. 12 (2001) 1191–1205.

[5] D. Dodou, P. Breedveld, P.A. Wieringa, Mucoadhesives in the gastrointestinal tract: revisiting the literature for novel applications, Eur. J. Pharm. Biopharm 60 (2005) 1–16.

[6] L. Serra, J. Doménech, N.A. Peppas, Engineering design and molecular dynamics of mucoadhesive drug delivery systems as targeting agents, Eur. J. Pharm. Biopharm 71 (2009) 519–528.

[7] J. Saurí, D. Millán, J.M. Suñé-Negre, P. Pérez-Lozano, R. Sarrate, A. Fàbregas, C. Carrillo, M. Miñarro, J.R. Ticó, E. García-Montoya, The use of the SeDeM diagram expert system for the formulation of Captopril SR matrix tablets by direct compression, Int. J. Pharm. 461 (2014) 38–45.

[8] J. Saurí, D. Millán, J.M. Suñé-Negre, H. Colom, J.R. Ticó, M. Miñarro, P. Pérez-Lozano, E. García-Montoya, Quality by Design approach to understand the physicochemical phenomena involved in controlled release of captopril SR matrix tablets, Int. J. Pharm. 477 (2014) 431–441.

[9] J. Saurí, J.M. Suñé-Negre, J. Díaz-Marcos, J. Vilana, D. Millán, J.R. Ticó, M. Miñarro, P. Pérez-Lozano, E. García-Montoya, Relationships between surface free energy, surface texture parameters and controlled drug release in hydrophilic matrices, Int. J. Pharm. 478 (2015) 328–340.

[10] J. Saurí, Doctoral Thesis, Desenvolupament i caracterització de comprimits matricials hidròfils de captopril, 2015. http://hdl.handle.net/10803/316030. Accessed 02/October/2015.

[11] A.O. Nur, J.S. Zhang, Recent progress in sustained/controlled oral delivery of captopril: an overview, Int. J. Pharm. 194 (2000) 139–146.

[12] M. Hu, G.L. Amidon, Passive and carrier-mediated intestinal absorption components of captopril, J. Pharm. Sci. 77 (1988) 1007–1011.

[13] S. Wu, Polar and nonpolar interactions in adhesion, J. Adhes. 5 (1973) 39–55.

[14] O. Planinsek, R. Pisek, A. Trojak, S. Srcic, The utilization of surface free-energy parameters for the selection of a suitable binder in fluidized bed granulation, Int. J. Pharm. 207 (2000) 77–88.

[15] C.M. Lehr, H.E. Boddé, J.A. Bouwstra, H.E. Junginger, A surface energy analysis of mucoadhesion II, Prediction of mucoadhesive performance by spreading coefficients, Eur. J. Pharm. Sci. 1 (1993) 19–30.

[16] G. Buckton, Bioadhesion and mucoadhesion, in: G. Buckton (Ed.), Interfacial Phenomena in Drug Delivery and Targeting, Harwood Academic Publishers, Switzerland, 1995, pp. 223–236.

[17] K.S. Cole, R.H. Cole, Dispersion and absorption in dielectrics I, alternating current characteristics, J. Chem. Phys. 9 (1941) 341–352.

[18] F. Kremer, A. Schönhals, Broadband Dielectric Spectroscopy, Springer, 2003. Berlin.

[19] H.K. Stulzer, P.O. Rodrigues, T.M. Cardoso, J.S.R. Matos, M.A.S. Silva, Compatibility studies between captopril and pharmaceutical excipients used in tablets formulations, J. Therm. Anal. Calorim. 91 (2008) 323–328.

[20] T. Gonçalves-Araújo, A.R. Rajabi-Siahboomi, I. Caraballo, Polymer percolation threshold in HPMC extended release formulation of carbamazepine and verapamil HCl, dSciTech 2 (2010) 558–562.

[21] C. Maderuelo, A. Zarzuelo, J.M. Lanao, Critical factors in the release of drugs from sustained release hydrophilic matrices, J. Control Release 154 (2011) 2–19.

[22] H. McPhillips, D.Q.M. Craig, P.G. Royall, V.L. Hill, Characterisation of the glass transition of HPMC using modulated temperature differential scanning calorimetry, Int. J. Pharm. 180 (1999) 83–90.

[23] A. Gómez-Carracedo, C. Alvarez-Lorenzo, J.L. Gómez-Amoza, A. Concheiro, Chemical structure and glass transition temperature of non-ionic cellulose ethers: DSC, TMDSC oscillatory rheometry study, J. Therm. Anal. Calorim. 73 (2003) 587–596.

[24] R. Macovez, E. Mitsari, M. Zachariah, M. Romanini, P. Zygouri, D. Gournis, J.Ll Tamarit, Ultraslow dynamics of water in organic molecular solids, J. Phys. Chem. C 118 (2014) 4941–4950.

[25] P. Tripathi, J. Gonzalo-Ruiz, E. Mitsari, M. Zachariah, M. Romanini, J.Ll Tamarit, F.X. Muñoz, R. Macovez, Silicon-chip-based dielectric spectroscopy for conductivity and molecular dynamics studies of organic films, J. Phys. Chem. Lett. 5 (2014) 2796–2801.

[26] M. Zachariah, M. Romanini, P. Tripathi, J.Ll Tamarit, R. Macovez, Molecular diffusion and dc conductivity perfectly correlated with molecular rotational dynamics in a plastic crystalline electrolyte, Phys. Chem. Chem. Phys. 17 (2015) 16053–16057.

[27] M. Zachariah, M. Romanini, P. Tripathi, M. Barrio, J.Ll Tamarit, R. Macovez, Self-diffusion, phase behavior, and Li+ ion conduction in succinonitrile-based plastic co-crystals, J. Phys. Chem. C 119 (2015) 27298–27306.

[28] R. Macovez, M. Zachariah, M. Romanini, P. Zygouri, D. Gournis, J.Ll Tamarit, Hopping conductivity and polarization effects in a fullerene derivative salt, J. Phys. Chem. C 118 (2014) 12170–12175.

[29] M. Zachariah, E. Mitsari, M. Romanini, P. Zygouri, D. Gournis, M. Barrio, J.Ll Tamarit, R. Macovez, Water-triggered conduction mediated by proton exchange in a hygroscopic fulleride and its hydrate, J. Phys. Chem. C 119 (2014) 685–694.